Radiology

MRI of the Internal Auditory Canal, Labyrinth, and Middle Ear: How We Do It

John C. Benson, MD • Matthew L. Carlson, MD • John I. Lane, MD

From the Departments of Radiology (J.C.B., J.I.L.) and Otolaryngology-Head and Neck Surgery (M.L.C.), Mayo Clinic, 200 1st St SW, Rochester, MN 55905. Received April 22, 2020; revision requested May 28; revision received June 4; accepted June 22. **Address correspondence to** J.C.B. (e-mail: *Benson.john3@mayo.edu*).

Conflicts of interest are listed at the end of this article.

Radiology 2020; 297:252–265 • https://doi.org/10.1148/radiol.2020201767 • Content codes: HN MR

MRI is firmly established as an essential modality in the imaging of the temporal bone and lateral skull base. It is used to evaluate normal anatomic structures, evaluate for vestibular schwannomas, assess for inflammatory and/or infectious processes, and detect residual and/or recurrent cholesteatoma. It is also extensively used in pre- and postoperative evaluations, particularly in patients with vestibular schwannomas and candidates for cochlear implantation. Nevertheless, despite the widespread use of MRI for these purposes, many radiologists remain unfamiliar with the complex anatomy and expected imaging findings with such examinations. The purpose of this review is to provide an overview of the most useful MRI sequences for internal auditory canal and labyrinthine imaging, review the relevant anatomy, and discuss the expected appearances of the most commonly encountered pathologic entities. In addition, the features at pre- and postprocedural MRI will be discussed to help ensure that diagnostic radiologists may be of greatest use to the ordering physicians.

Online SA-CME • *See www.rsna.org/learning-center-ry*

Learning Objectives:

After reading the article and taking the test, the reader will be able to:

- Identify the major anatomic structures visible on MRI within the internal auditory canal (IAC), labyrinth, and middle ear
- Describe the poor prognostic imaging features of vestibular schwannomas
- Describe the typical MRI appearance of acute labyrinthitis and labyrinthitis ossificans

Accreditation and Designation Statement

The RSNA is accredited by the Accreditation Council for Continuing Medical Education (ACCME) to provide continuing medical education for physicians. The RSNA designates this journal-based SA-CME activity for a maximum of 1.0 *AMA PRA Category 1 Credit*™. Physicians should claim only the credit commensurate with the extent of their participation in the activity.

Disclosure Statement

The ACCME requires that the RSNA, as an accredited provider of CME, obtain signed disclosure statements from the authors, editors, and reviewers for this activity. For this journal-based CME activity, author disclosures are listed at the end of this article.

MRI of the temporal bone and lateral skull base has become a mainstay of neuroradiology to delineate anatomic structures and to investigate neoplastic or infectious processes affecting this complex space. Common applications of MRI include diagnostic evaluation of sensorineural hearing loss, assessment of cochlear implant candidacy, monitoring for residual or recurrent cholesteatoma within the tympanomastoid space, and monitoring for vestibular schwannoma within the inner auditory canal or cerebellopontine angle. In many cases, MRI is complementary to CT in the evaluation of surgical candidates, such as individuals being considered for pediatric cochlear implantation, where the labyrinth may be malformed and the facial nerve may take an anomalous course through the temporal bone.

Radiologists who interpret such imaging studies should be well-versed in the expected appearances of the most common pathologic entities. Herein, we outline the most useful MRI sequences, review the imaging characteristics of the most frequently encountered pathologic entities, and describe the use of MRI in the postoperative follow-up of vestibular schwannomas and cholesteatomas.

MRI Technique

Our institution conducts the vast majority of internal auditory canal (IAC) MRI examinations with 3-T magnets, which allow for a superior signal-to-noise ratio and higher spatial resolution compared with 1.5-T imaging. In addition, 3-T imaging can be completed with shorter acquisition times. Such benefits are not without costs, as 3-T images contain more banding and susceptibility artifacts, particularly with gradient-recalled echo sequences (1). In recent years, pioneering work has introduced 7-T imaging for IAC evaluations. Such imaging yields further increases in signal-to-noise ratio and spatial resolution at the expense of even more degradation by susceptibility artifacts (2,3). The use of parallel transmit techniques may help overcome the signal drop-off in the posterior fossa and IAC on 7-T images; we are currently assessing the capabilities of this technique.

Our institution uses multichannel phased-array coils to substantially increase the signal-to-noise ratio of acquired images. Currently, we use either a 32- or 64-channel head coil, depending on what is available for each scanner's platform. A dedicated multichannel head coil achieves an excellent signal-to-noise ratio of the cerebellopontine angle. It is also capable of producing high spatial resolution of cranial nerves VII and VIII, even with 1.5-T scanners.

Like most other institutions, ours has made small field-of-view T2-weighted cisternography the workhorse MRI sequence for imaging the IAC and associated anatomic

Abbreviations

FLAIR = fluid-attenuated inversion recovery, FSE = fast spin echo, IAC = internal auditory canal, SPACE = sampling perfection with application-optimized contrasts by using flip angle evolution, 3D = three-dimensional

Summary

MRI of the inner auditory canal, middle ear, and labyrinth is complex and requires a detailed knowledge of the regional anatomy, the most common pathologic entities, and the expected postsurgical findings.

Essentials

- MRI of vestibular schwannomas has prognostic value and is used to guide surgical approaches.
- Preoperative examinations of candidates for cochlear implants should be closely scrutinized for anatomic and pathologic conditions relevant to surgery.
- Non–echo-planar diffusion-weighted imaging is highly accurate in the diagnosis of residual and recurrent cholesteatomas.
- Early detection of labyrinthitis is crucial so that cochlear implantation can be performed if indicated, before labyrinthitis ossificans ensues.

structures. Both three-dimensional (3D) gradient-recalled echo (eg, constructive interference in steady state, or CISS, from Siemens [Erlangen, Germany] and fast imaging employing steady-state acquisition, or FIESTA, from GE Healthcare [Chicago, Ill]) and 3D fast spin-echo (FSE) options are available (4). Although both are routinely used, we prefer 3D FSE (T2-weighted sampling perfection with application-optimized contrasts using flip angle evolution [SPACE] from Siemens) because it eliminates banding artifact, has less flow artifact, and has less susceptibility artifact produced at the air-bone interfaces of the skull base (5,6). The banding artifact is particularly problematic when examining the labyrinth, particularly at 3 T. Comparative analyses have shown 3D FSE imaging to be superior at demonstrating the cranial nerves and labyrinthine structures (7). We routinely include coronal reconstructions of the axially acquired 3D T2-weighted FSE images. In cases of preoperative pediatric cochlear implant evaluation where the integrity of the cochlear nerve may be in question, we acquire direct oblique sagittal volumes through the IACs to provide the best spatial resolution possible.

Likewise, we favor 3D FSE over 3D gradient-recalled echo volumetric breath-hold examination for T1-weighted images. The major difference between these two techniques is that of flow-related enhancement. The enhancement signal intensity is present within the adjacent major vascular structures on 3D gradient-recalled echo images but is nullified on 3D FSE images. Furthermore, 3D FSE T1-weighted imaging is better able to depict the fluid-filled labyrinthine structures within the backdrop of the densely ossific otic capsule. Three-dimensional gadolinium-enhanced T2-weighted SPACE fluid-attenuated inversion recovery (FLAIR) images are used to evaluate for subtle alterations in labyrinthine fluid signal intensity that are undetectable on 3D FSE T2-weighted SPACE images.

The use of 3D techniques for our small field-of-view sequences provides substantial benefits over two-dimensional techniques. Most notably, the isometric voxels produced with 3D imaging allow for multiplanar reconstructions, which are particularly useful in evaluating the cisternal and canalicular portions of cranial nerves VII and VIII for pediatric cochlear implantation. However, the longer acquisition times necessary for 3D imaging makes such sequences vulnerable to motion artifact. The only two-dimensional acquisition within our standard IAC protocol is whole-brain axial T2-weighted FLAIR (Table).

We routinely use fat saturation on contrast material–enhanced images to differentiate pathologic enhancement from intrinsically T1 hyperintense structures such as lipid-rich bone marrow. Differentiation of these areas is of particular importance after translabyrinthine surgical resection of vestibular schwannomas, where surgeons use a large fat graft to obliterate the mastoid to reduce the risk of cerebrospinal fluid leak. Fat saturation helps differentiate residual tumor from the fat graft. In some cases, fat saturation can also help narrow the differential of cerebellopontine angle masses, for example with dermoid cysts, lipomas, and cholesterol granuloma (Fig 1) (8,9).

Summary of Parameters for 3-T MRI of the Internal Auditory Canal

Parameter	Axial T2-weighted FLAIR with Fat Saturation	Axial T2-weighted SPACE	Axial T1-weighted SPACE	Axial T1-weighted Fat-saturated SPACE with Gadolinium-based Contrast Material	Axial T2-weighted FLAIR SPACE with Gadolinium-based Contrast Material
TR (msec)	9000	1300	600	600	5000
TE (msec)	118	184	32	32	379
Data matrix	224 × 320	320 × 320	192 × 192	192 × 192	192 × 192
FOV (mm)	220	150	150	150	150
No. of signals acquired	1	2	2	2	2
Bandwidth (Hz)	287	651	651	651	651
Voxel size (mm^3)	1.2 × 0.9 × 4.0	0.5 × 0.5 × 0.8	0.8 × 0.8 × 0.9	0.8 × 0.8 × 0.9	0.8 × 0.8 × 1.6
Flip angle (°)	180	120	…	…	…
Imaging duration	4 minutes 32 seconds	3 minutes 55 seconds	4 minutes	4 minutes	4 minutes 29 seconds

Note.—FLAIR = fluid-attenuated inversion recovery, FOV = field of view, SPACE = sampling perfection with application-optimized contrasts by using flip angle evolution, TE = echo time, TR = repetition time.

To assess for residual or recurrent cholesteatomas, we add axial and coronal diffusion-weighted imaging to our IAC imaging protocol, as the lesions demonstrate intense restricted diffusion due to their high keratin content. Specifically, non–echo planar diffusion-weighted imaging is used, which is less prone to susceptibility artifact and is capable of thin-slice imaging, and consequently outperforms echo-planar imaging (10,11). Focal restricted diffusion is highly specific for recurrent cholesteatomas, and lesions as small as 2 mm in diameter can be detected. Lower-resolution diffusion sequences can be coregistered with higher-resolution MRI sequences or multidimensional CT to better delineate the anatomic location of the cholesteatoma recurrence (12).

Normal IAC Anatomy

The anatomy of the IAC is best demonstrated on high-resolution T2-weighted images, reformatted in a parasagittal oblique plane perpendicular to the IAC. The IAC contains the facial nerve, vestibulocochlear nerve, nervus intermedius, and labyrinthine artery. The vestibulocochlear nerve exits the brainstem as a single large nerve just posterosuperior to the facial nerve and then divides into the cochlear, superior, and vestibular nerves near the porus acusticus. In the majority of patients, 3-T imaging will also demonstrate the nervus intermedius that exits the brainstem lateral to the motor root of the facial nerve and travels along the posterior aspect of cranial nerve VII until joining the facial nerve just proximal to the meatal foramen at the fundus of the IAC (Fig 2) (13). Within the lateral IAC, a transverse segment of bone named the falciform crest bisects the canal along its horizontal axis. The vertical segment of bone, termed the Bill bar, separates the facial nerve from the superior vestibular nerve. A loop of the anterior inferior cerebellar artery also enters the IAC in 20%–40% of individuals and is generally of no clinical significance (14). The numerous small osseous foramina that arise from the IAC, such as the singular and fallopian canals, cochlear aperture, and tiny openings of the fundal cribiform plate, are typically better evaluated with CT (15).

The aptly named labyrinth is anatomically complex. The otic capsule is comprised of the dense temporal bone that forms the structure of the inner ear and is segmented into the semicircular canals, vestibule, and cochlea. This bony capsule contains the membranous labyrinth, which is made up of endolymph-containing ducts and sacs that are separated from the surrounding bone by perilymphatic fluid (16). Within the osseous vestibule are two membranous sacs that detect linear acceleration. One is called the utricle, which is located adjacent to the semicircular canals and innervated by the superior vestibular nerve. This sac detects horizontal linear acceleration. The other is the smaller saccule, which is located near the cochlea and innervated by the saccular branch of the inferior vestibular nerve. This sac detects vertical linear acceleration.

Within the semicircular canals are ducts by the same names. The superior and lateral semicircular ducts are innervated by the superior vestibular nerve, whereas the posterior semicircular canal is innervated by the inferior vestibular nerve. Despite the lateral semicircular canal being commonly referred to as the horizontal semicircular canal, its plane actually rests approximately 30° off the true horizontal. The ducts are focally dilated at one end in a region named the ampulla. Each ampulla contains a crista ampullaris, a cone-shaped sensory structure that deflects during movement of endolymph within the ducts, thereby sensing rotational movements. The crista ampullaris is sometimes detectable on high-resolution T2-weighted images and appears as a small low-signal-intensity focus within the ampulla.

The cochlea is made up of the scala media (also known as the cochlea duct) bordered by two perilymphatic channels called the scala tympani and scala vestibuli. The scala vestibuli transmits fluid waves from the oval window, whereas the scala tympani allows the pressure to decompress by propagating the wave to the round window; these meet at the helicotrema within the cochlea apex. Along the inner wall of the cochlear

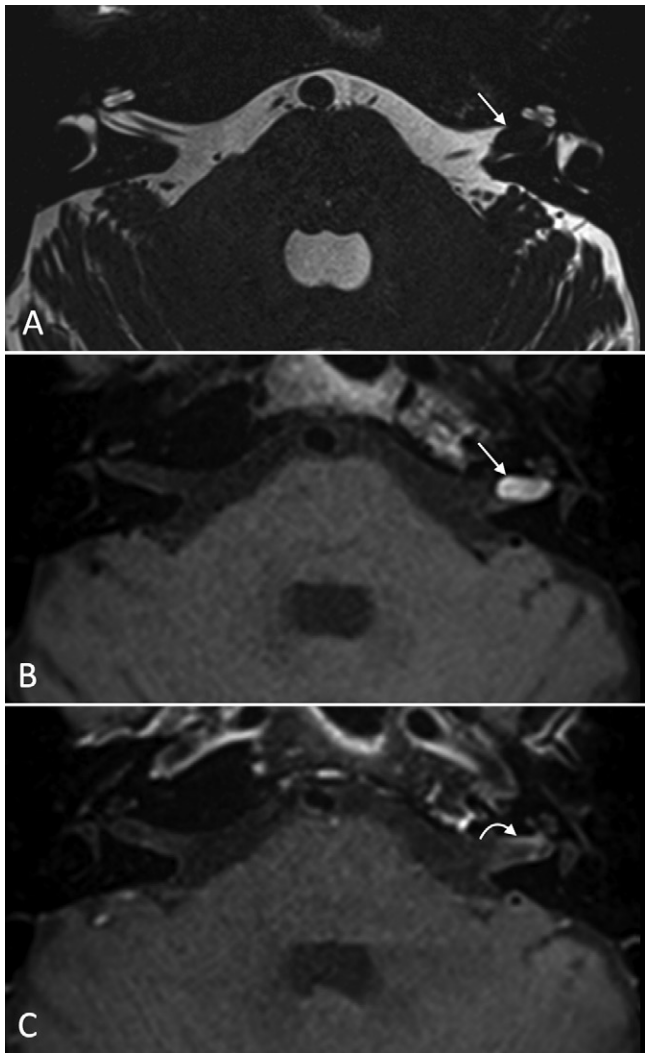

Figure 1: MRI scans of inner auditory canal (IAC) lipoma in a 54-year-old man demonstrate the usefulness of fat saturation. *A*, Axial T2-weighted sampling perfection with application-optimized contrasts by using flip angle evolution (SPACE) image demonstrates a well-circumscribed mass in the left IAC (arrow). *B*, Unenhanced T1-weighted SPACE image shows that the mass (arrow) has substantial intralesional T1 hyperintensity, which drops out on, *C*, fat-saturated contrast-enhanced T1-weighted SPACE image. Faint peripheral enhancement versus incomplete signal drop out is noted (arrow).

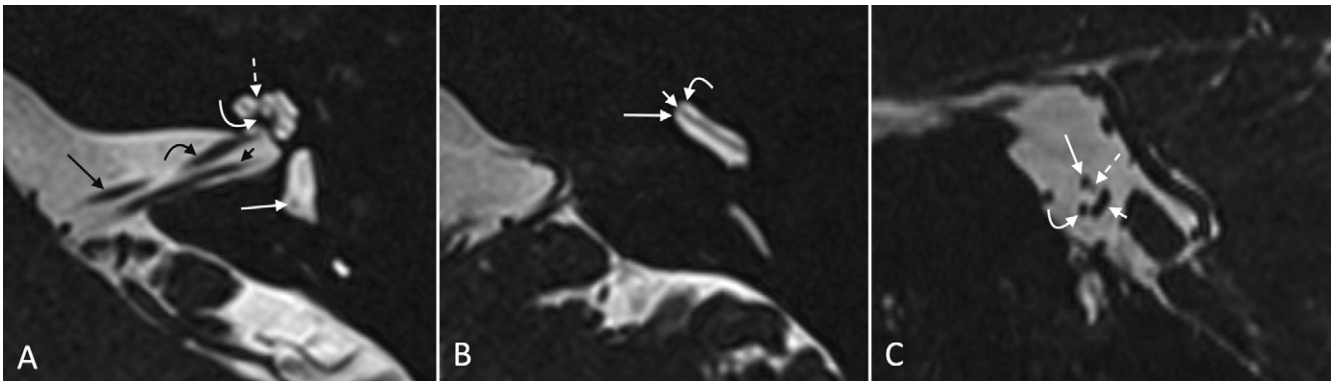

Figure 2: Normal inner auditory canal and labyrinthine anatomy in a 37-year-old woman. *A*, *B*, Axial and, *C*, reformatted oblique sagittal T2-weighted sampling perfection with application-optimized contrasts by using flip angle evolution (SPACE) MRI scans at 3 T show the expected appearance of the regional anatomic structures. *A*, On axial image, the facial nerve (long straight black arrow), cochlear nerve (curved black arrow), and inferior vestibular nerve (short black arrow) are all identified. Components of the cochlea, such as the interscalar septa (dashed white arrow) and modiolus (curved white arrow) are easily visualized. The crista ampullaris of the posterior semicircular canal (solid straight white arrow) is also seen. *B*, Within the cochlea, the spiral lamina/basilar membrane complex (short straight arrow) is seen as a clear border between the scala vestibuli (curved arrow) and scala tympani (long straight arrow), particularly within the basal turn of the cochlea. *C*, The nerves are often best seen on reformatted images. The facial nerve is located within the anterosuperior cerebellopontine angle (long straight solid arrow), while the cochlea nerve is located anteroinferiorly (curved arrow). The nervus intermedius is located just posterior to the facial nerve (dashed arrow). The superior and inferior divisions of the vestibular nerve are often indistinguishable at this point of the canal (short straight arrow).

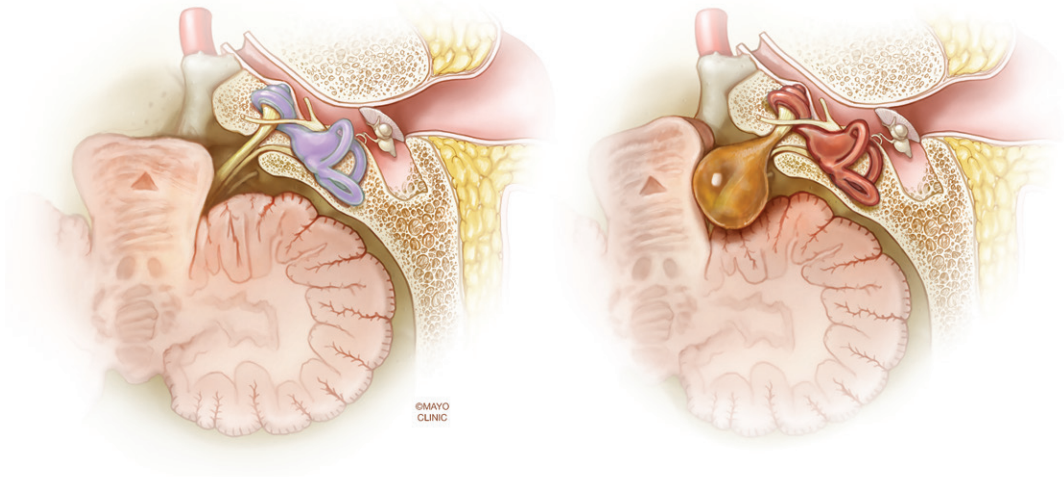

Figure 3: Illustration of fluid alterations within the membranous labyrinth in the setting of a vestibular schwannoma. The left image shows normal endolymphatic and perilymphatic fluid; the right image demonstrates a vestibular schwannoma extending into the inner auditory canal, with abnormal labyrinthine fluid. (Image used with permission of Mayo Foundation for Medical Education and Research, all rights reserved.)

spiral, the spiral lamina is usually discernable on 3-T images as a landmark between the scala vestibuli and tympani. Along the outer wall, however, the scala media lies between these structures, bordered by the Reissner membrane ventrally, the basilar membrane dorsally, and the spiral ligament and otic capsule laterally. Although the membranous borders of the scala media have been identified on high-resolution ex vivo MRI scans, they are not typically visualized on clinical 3-T images (17).

Recently it has been noted that gadolinium accumulates over time within the perilymph, leaving the endolymph visible as an unopacified fluid compartment within the bony labyrinth. A few studies have investigated the use of this technique to diagnose endolymphatic hydrops (18,19). Most of these imaging protocols used 3D FLAIR sequences 4–8 hours after intratympanic or intravenous gadolinium administration. However, the use of these techniques remains largely investigational, and they are not routinely employed in clinical practice at most institutions.

Vestibular Schwannomas

Imaging Characteristics

Vestibular schwannomas are benign nerve sheath tumors that arise from the vestibular portion of the eighth cranial nerve. Approximately 95% of tumors are unilateral and sporadic, while the rest of cases typically occur in the setting of neurofibromatosis type 2, which is a condition hallmarked by the development of bilateral vestibular schwannomas (20). Vestibular schwannomas comprise 6%–8% of intracranial tumors and

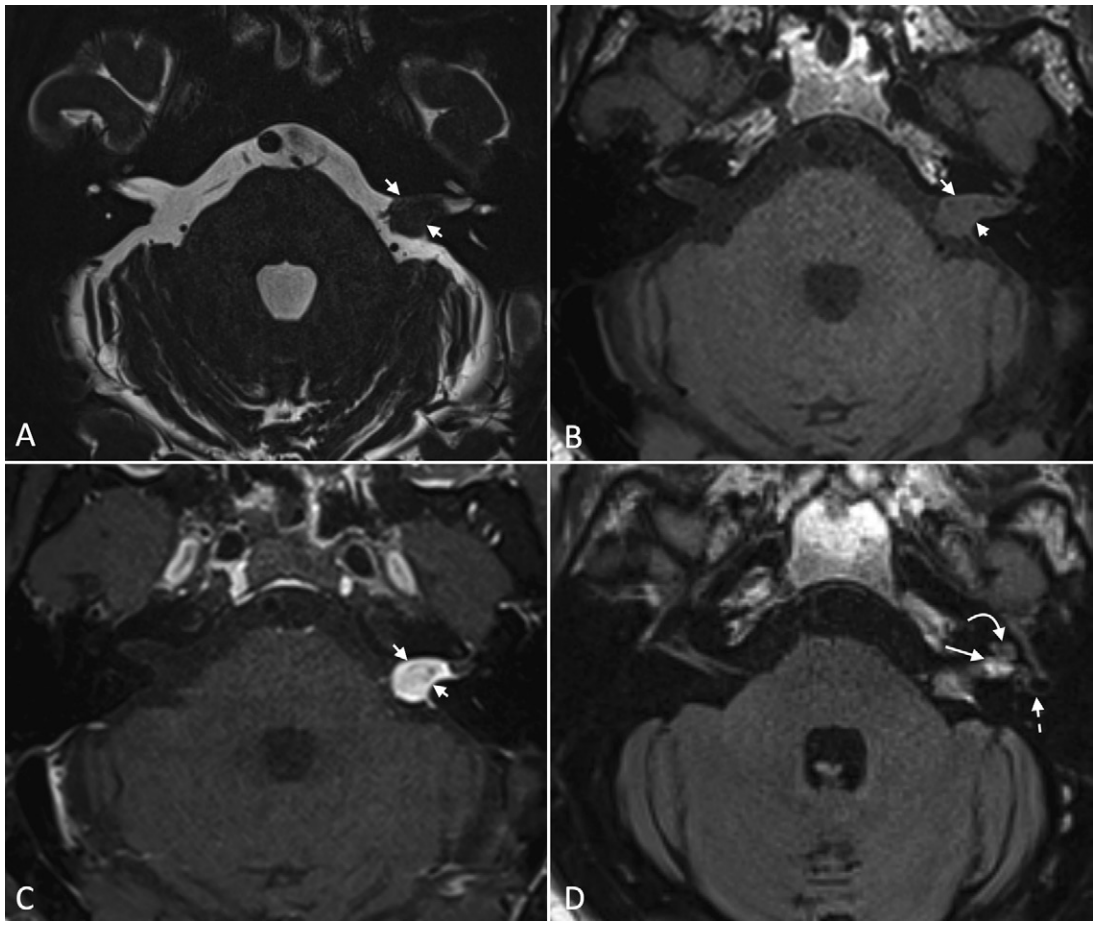

Figure 4: Abnormal fluid-attenuated inversion recovery (FLAIR) signal intensity associated with a vestibular schwannoma in a 67-year-old man. *A*, T2-weighted sampling perfection with application-optimized contrasts by using flip angle evolution (SPACE), *B*, T1-weighted SPACE, and, *C*, contrast-enhanced T1-weighted SPACE images demonstrate an avidly enhancing mass in the left inner auditory canal (IAC) that extends through the porus acousticus into the left cerebellopontine angle, compatible with a vestibular schwannoma (arrows). *D*, Three-dimensional T2-weighted FLAIR SPACE image shows abnormal hypertense fluid within the IAC fundus (straight solid arrow), cochlea (curved arrow), and lateral semicircular canal (dashed arrow).

more than 90% of cerebellopontine angle tumors. Owing to more widespread access to head MRI and greater adherence to screening protocols for asymmetric sensorineural hearing loss, the incidence of vestibular schwannomas has risen from 1.5 to 4.2 per 100 000 population per year in the past half-century (21,22). Approximately half of tumors will not grow for an extended period of time after initial diagnosis, and the average growth rate among growing tumors is approximately 1–2 mm per year (23). This slow growth rate has imaging implications in that detection of tumor growth will often require comparing the current study to images obtained at more than just one prior annual examination. In addition, volumetric assessment of tumor growth has been demonstrated to be a more sensitive measure of tumor growth than linear diameter assessment (23).

In general, vestibular schwannomas are easily recognizable on images. Compared with adjacent parenchyma, vestibular schwannomas are typically T1 isointense, T2 hyperintense, and avidly enhance with contrast agents. Intralesional cysts and hemorrhage are common, which may contribute to signal heterogeneity and blooming foci with T2*-weighted gradient-echo sequences. Larger tumors often lead to bony remodeling and/or enlargement of the IAC and/or porus acousticus and compression of the adjacent cerebellum, cerebellar peduncles, or brainstem (Fig 3).

Many imaging features of vestibular schwannomas have prognostic value. Not surprisingly, patients with smaller and slower-growing tumors fare better in terms of maintaining serviceable hearing (24). The presence of cerebrospinal fluid located lateral to the tumor within the IAC is associated with better hearing outcomes after surgery (25). Vestibular schwannomas arising from the superior vestibular nerve also have more favorable prognoses in terms of hearing preservation. Cystic tumors, which are composed primarily of large coalescent cysts, are generally faster growing with a shorter clinical history and often treated as more aggressive lesions (26).

Signal intensity alterations exist within the ipsilateral inner ear in patients with vestibular schwannomas. Specifically, FLAIR signal intensity is increased within the perilymphatic fluid, which normally is suppressed with such sequences (Fig 4) (27). The perilymph has long been known to have elevated protein levels in the presence of vestibular schwannomas (labyrinthine taps were used to test for this before nonenhanced CT and MRI), and this proteinaceous fluid has been hypothesized

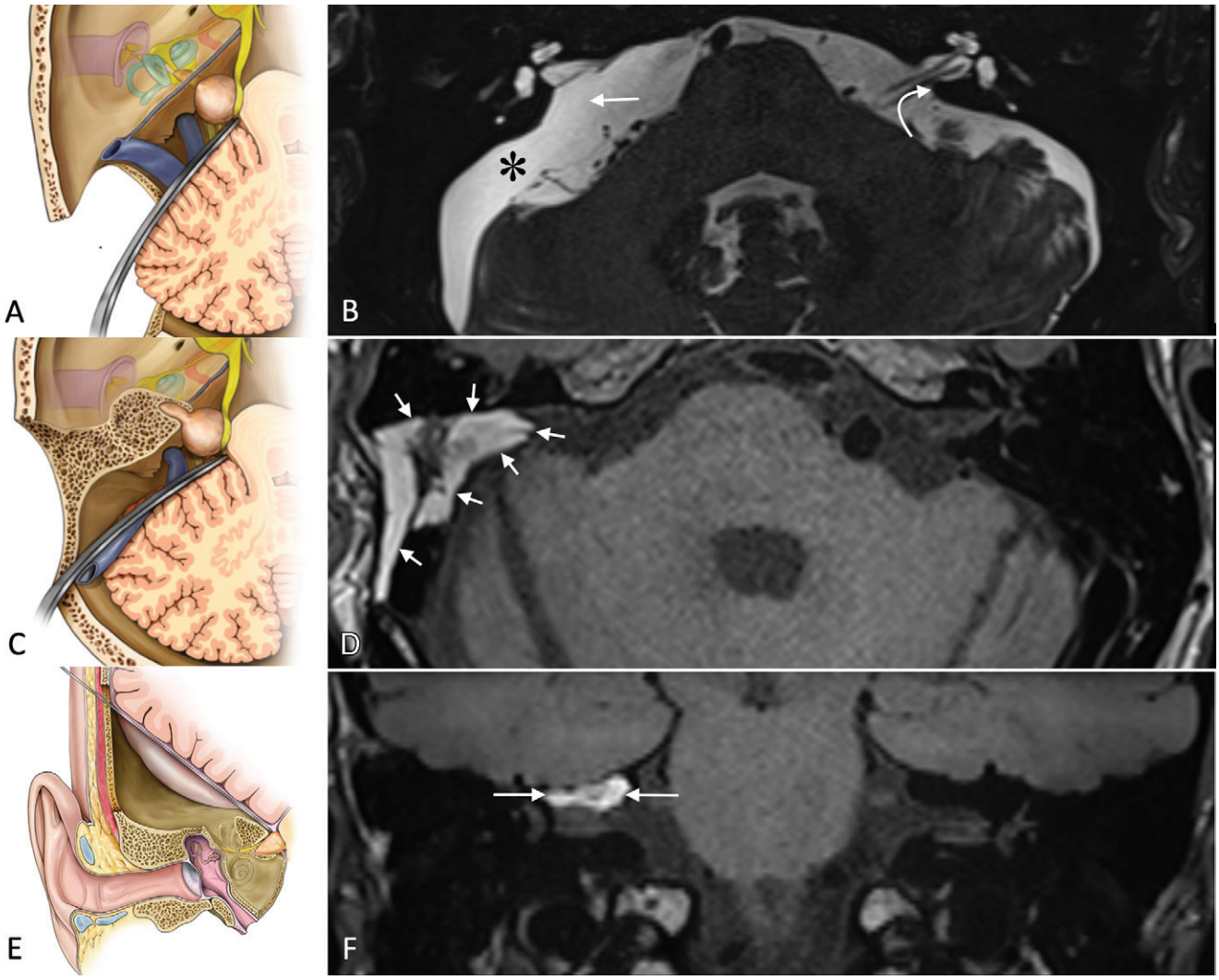

Figure 5: Illustrations and corresponding postoperative MRI scans of the three primary surgical approaches used for resection of vestibular schwannoma. *A*, The retrosigmoid (suboccipital) approach is performed though an occipital craniotomy placed just posterior and inferior to the sigmoid-transverse junction. The cerebellum is retracted and then bone is removed over the medial two-thirds of the internal auditory canal. *B*, Postoperative scan demonstrates surgical absence of the posterior wall of the right inner auditory canal (straight arrow); the contralateral side is shown for comparison (curved arrow). Extra-axial fluid related to surgical retraction (*) overlies the right cerebellar hemisphere. *C*, The translabyrinthine approach entails a wide mastoidectomy, decompression of the sigmoid sinus, labyrinthectomy, and bone removal over the internal auditory canal and presigmoid posterior fossa dura to expose the tumor. *D*, Postoperative T1-weighted image demonstrates the fat graft within the postoperative site (arrows). *E*, The middle cranial fossa approach involves a temporal craniotomy with subtemporal extradural brain retraction. The bone overlying the internal auditory canal is then drilled to access the tumor. *F*, Coronal postoperative image demonstrates the fat graft laid along the roof of the right inner auditory canal (arrows). (Image used with permission of Mayo Foundation for Medical Education and Research, all rights reserved.)

as the explanation for such signal intensity abnormalities (28). The clinical significance of the increased FLAIR signal intensity remains uncertain. Some studies have failed to demonstrate an association between the change in signal intensity and the severity of hearing loss (29). Others have found such an association and have suggested that high signal intensity portends a poor prognosis for regaining hearing (30,31). Nevertheless, because intralabyrinthine FLAIR signal intensity changes remain a notable ancillary finding and a topic of continued interest, our institution routinely incorporates 3D FLAIR sequences into our IAC protocol partly to assess for such changes.

Preoperative Evaluation

The goal of microsurgery is maximal resection with preservation of neurologic function (32). Historically, gross total resection was highly prioritized. However, in more recent years aggressive subtotal resection has been used with increasing frequency to preserve facial nerve function. Three types of surgical approaches are used to resect vestibular schwannomas: translabyrinthine, middle cranial fossa, and retrosigmoid (Fig 5). The primary determinants of surgical approach choice are baseline hearing capacity, tumor size, tumor location, and patient age. The middle cranial fossa and retrosigmoid approaches spare the labyrinth and may be used in patients with good baseline hearing, where hearing preservation surgery is a realistic goal. The middle cranial fossa approach is generally reserved for small intracanalicular tumors in patients with good preoperative hearing levels. In contrast, the retrosigmoid approach can be used for any size tumor, ranging from a small medial-based intracanicular tumor to a large 5-cm tumor. Although controversial, there are some nuances when choosing

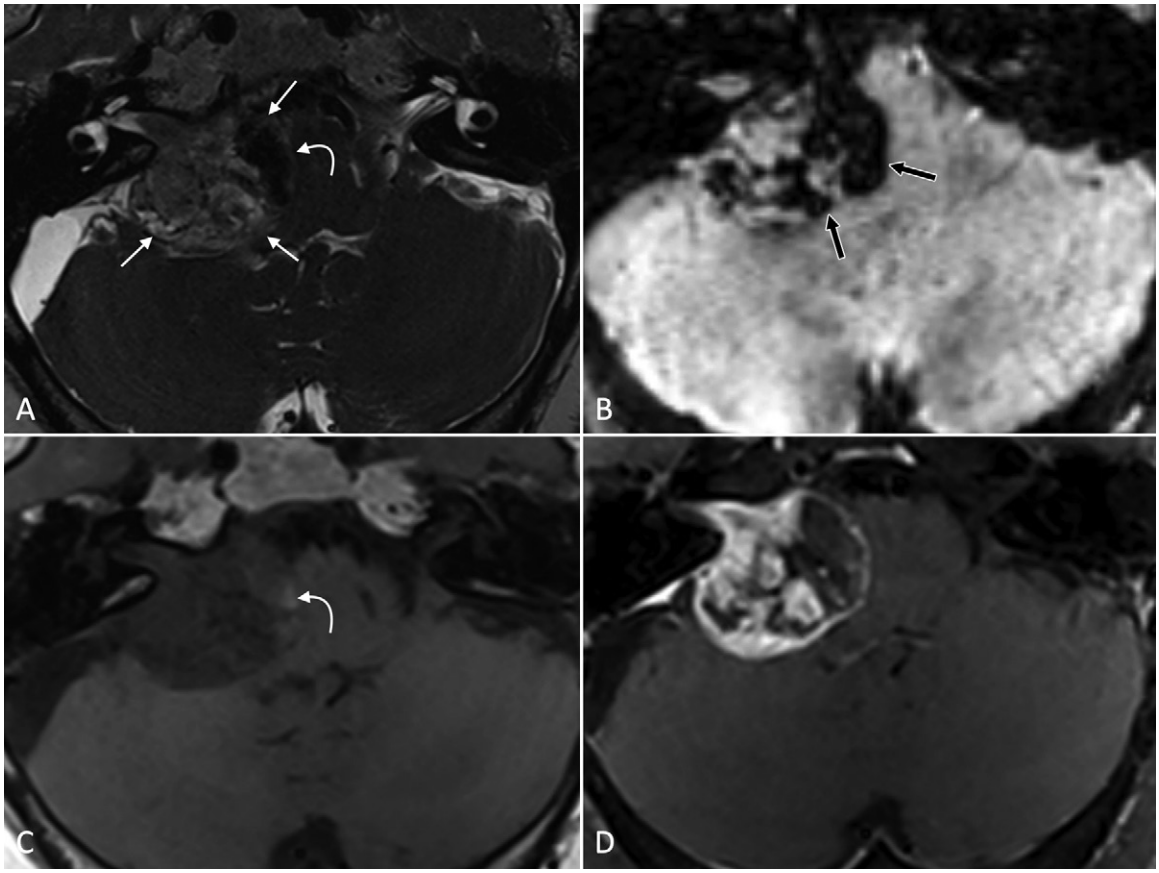

Figure 6: Images of hemorrhagic vestibular schwannoma in a 79-year-old man. *A*, *B*, Axial T2-weighted sampling perfection with application-optimized contrasts by using flip angle evolution (SPACE) images show a large vestibular schwannoma in the right cerebellopontine angle and internal auditory canal (straight arrows in *A*). Hypointense T2 signal along the lesion's medial margin (curved arrow in *A*) and blooming intralesional signal intensity on susceptibility-weighted image (arrows in *B*) are compatible with intratumoral hemorrhage. Similarly, hyperintense T1 signal within the vestibular schwannoma on, *C*, T1-weighted SPACE image (arrow) is consistent with hemorrhage and is differentiated from tumoral enhancement seen on, *D*, contrast-enhanced T1-weighted SPACE image.

between these two approaches, such as a greater short-term headache risk with the retrosigmoid approach and a greater short-term risk of facial paralysis with the middle cranial fossa approach. In contrast, the translabyrinthine approach by definition sacrifices hearing because the semicircular canals and vestibule are drilled through during the approach. The translabyrinthine approach is often used to resect the vestibular schwannoma in patients with poor baseline hearing or in those with large tumors, where hearing preservation surgery is not realistically feasible.

Furthermore, decisions regarding the treatment of vestibular schwannomas are complex and multifaceted beyond those of surgical approaches. The most common management options—observation, stereotactic radiosurgery, and surgical resection—must be considered in the context of existing neurologic function, tumor size, patient age, comorbidities, and patient preference (33). Conservative management is often initially employed for tumors smaller than 1.5 cm in the cerebellopontine angle (34). Tumors larger than 1.5 cm or those that exhibit growth at serial imaging are frequently treated with either radiosurgery or microsurgical resection, whereas resection is preferred for those larger than 2.5 cm. Familiarity with these treatment approaches is essential for radiologists to play a role in the multidisciplinary management of vestibular schwannomas.

Preoperative imaging helps to both aid in the decision of surgical approach and assess the regional anatomy. In retrosigmoid approach operations, the IAC is accessed by drilling through the posterior meatal lip and decompressing the medial two-thirds of the IAC. Preprocedural planning for this depends on assessing the relationship between the dural sinuses, labyrinth, and tumor. As a general rule, the lateral third of the IAC cannot be directly visualized with the retrosigmoid approach when attempting to preserve hearing; drilling more lateral will risk entry into the vestibule and posterior semicircular canal with resultant hearing loss. Some surgeons advocate using the endolymphatic duct as a reliable surgical landmark while decompressing the IAC for tumor resection when hearing preservation is being attempted. Specifically, if the surgeon is able to stay just medial to the endolymphatic duct, surgical exposure can be maximized without inadvertently drilling into the labyrinth and causing profound hearing loss. Remarkably, most data indicate that drilling along the medial edge of this structure does not incur substantial risk of hearing loss (35).

Preoperative radiology reports should contain information pertinent to future treatment planning. A high-riding jugular bulb should be noted, as it may impede surgical access to the

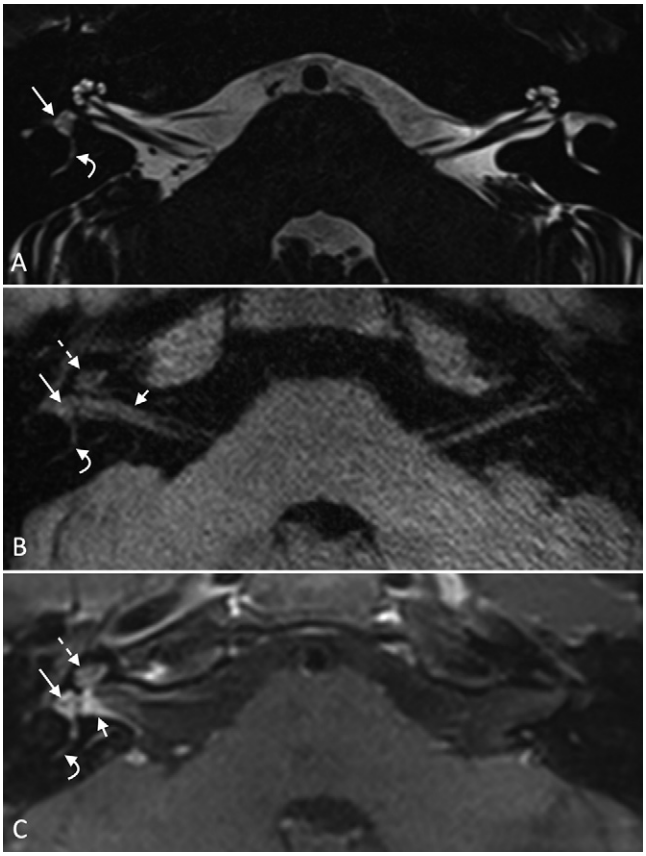

Figure 7: Acute labyrinthitis in an 18-year-old man with sudden-onset right-sided sensorineural hearing loss. *A*, T2-weighted sampling perfection with application-optimized contrasts by using flip angle evolution (SPACE) image demonstrates slightly decreased signal intensity within the vestibule (straight arrow) and lateral semicircular canal (curved arrow). *B*, Fluid-attenuated inversion recovery and, *C*, contrast-enhanced T1-weighted SPACE images show much more extensive involvement, with signal intensity alteration and enhancement also within the cochlea (dashed arrow) and along the canalicular segments of the nerves and dural surfaces within the inner auditory canal (short straight solid arrow), along with signal. Long straight solid arrow indicates the vestibule, and curved arrow indicates the lateral semicircular canal.

intrameatal components of a vestibular schwannoma during retrosigmoid operations. Similarly, a high-riding jugular bulb or anteriorly located sigmoid sinus may limit the surgical corridor with the translabyrinthine approach. Intralesional hemorrhage should be described, as hemorrhagic vestibular schwannomas are prone to causing abrupt changes in neurologic function (Fig 6) (36). Finally, preprocedural imaging can help assess for findings that put patients at higher risk for postoperative complications (37). Pneumatization of the temporal bone adjacent to the IAC is a risk factor for cerebrospinal fluid leak, whereas a loop of anterior inferior cerebellar artery adherent to the posterior petrous dura may risk vascular injury. In addition, the presence of chronic ear disease should make surgeons wary of seeding deeper infections (37).

Postoperative Evaluation and Follow-up

The expected postoperative imaging findings are dependent on the surgical method employed. Middle cranial fossa approach surger-

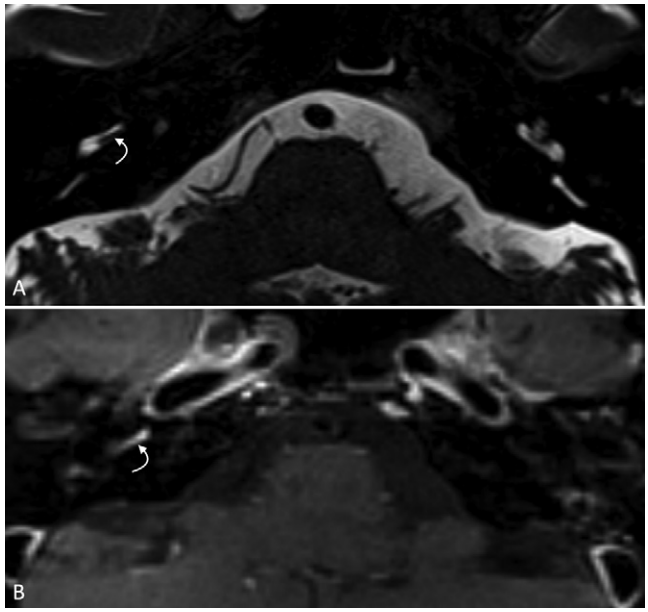

Figure 8: Intralabyrinthine schwannoma in a 72-year-old man with a history of predominantly right-sided sensorineural hearing loss. *A*, Axial T2-weighted sampling perfection with application-optimized contrasts by using flip angle evolution (SPACE) image demonstrates a hypointense mass in the scala tympani of the basal turn of the cochlea (arrow). *B*, Contrast-enhanced T1-weighted SPACE image shows that the lesion (arrow) avidly enhances and is compatible with an intralabyrinthine schwannoma.

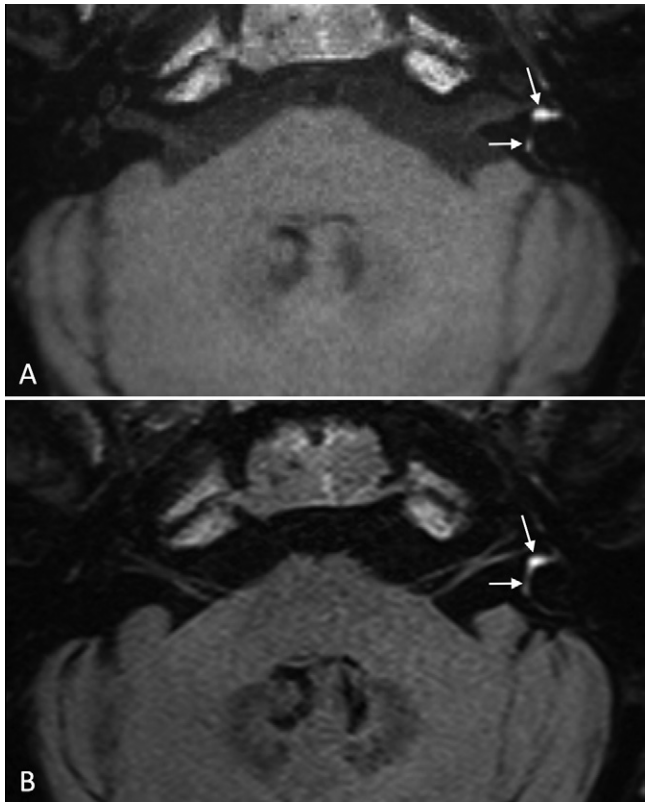

Figure 9: Idopathic intralabyrinthine hemorrhage in a 72-year-old man who presented with sudden left-sided sensorineural hearing loss. Axial, *A*, T1-weighted and, *B*, T2-weighted sampling perfection with application-optimized contrasts by using flip angle evolution, or SPACE, images demonstrate intrinsic T1 and T2 hyperintense signal intensity within the utricle and adjacent semicircular canals (arrows), compatible with blood products.

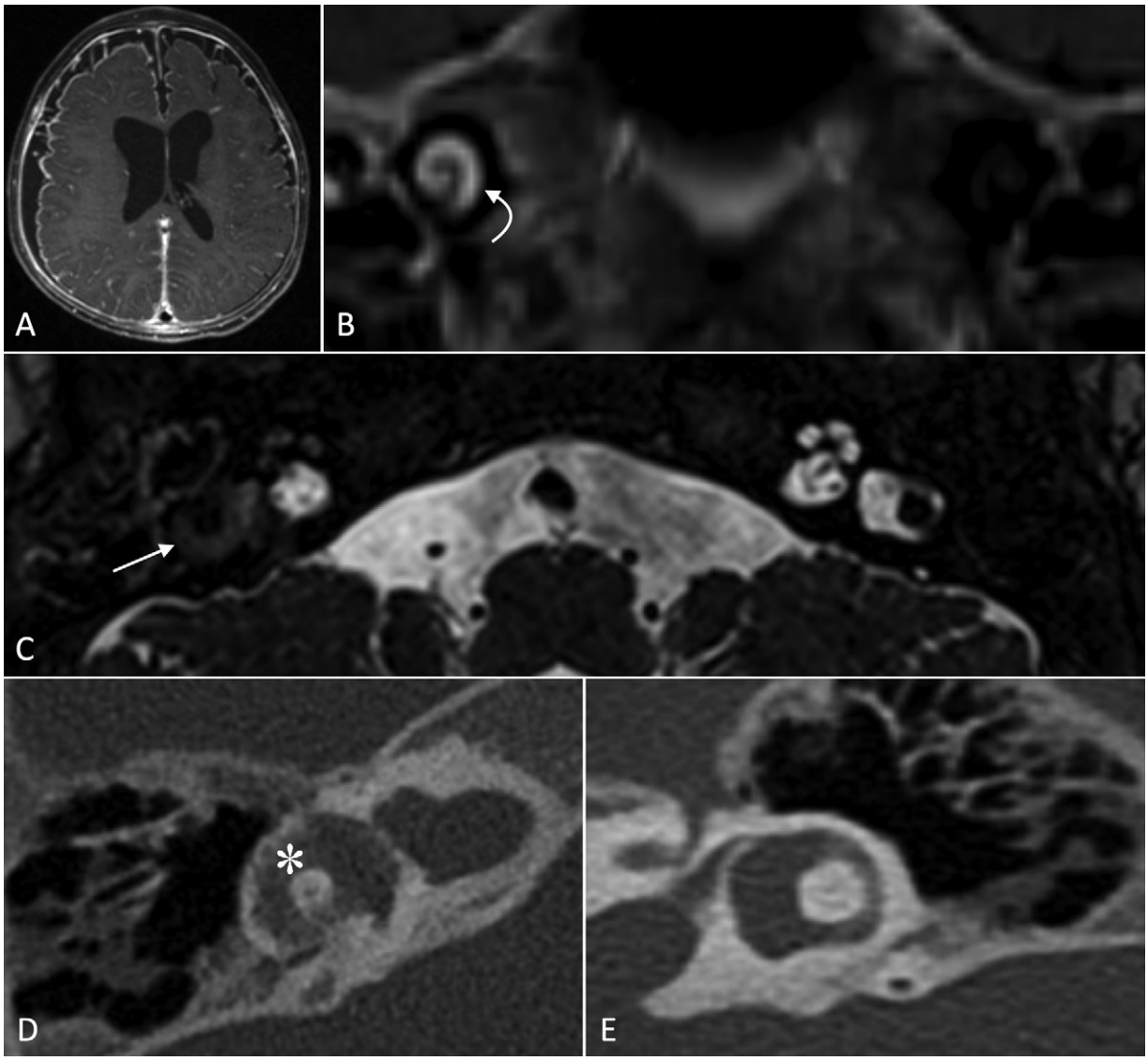

Figure 10: *A*, Axial contrast-enhanced MRI scan of the brain shows labyrinthitis ossificans in an 8-month-old boy who developed streptococcal meningitis, which was complicated by subdural empyemas. *B*, *C*, MRI scans obtained 1 month later demonstrate avid enhancement and decreased T2 signal intensity within the labyrinthine structures, including the cochlea (arrow in *B*) and lateral semicircular canal (arrow in *C*). *D*, Temporal bone CT scan obtained after MRI demonstrates resorption of the walls of the lateral semicircular canal with faint internal ossification (*). *E*, Temporal bone CT scan of the normal left side is shown for comparison.

ies require intraoperative retraction of the temporal lobe, which may lead to encephalomalacia, gliosis, and, much less commonly, symptomatic seizures or aphasia. In addition, surgeons access the IAC during a middle cranial fossa approach resection by drilling down through its roof. A fat or muscle graft is then often set at the site of the drilling, which is conspicuous on postoperative T1-weighted images. Fat packing after a translabyrinthine surgery, conversely, will be far more extensive and centered within the mastoidectomy cavity. Retrosigmoid surgeries require medial retraction of the ipsilateral cerebellar hemisphere and, consequently, can often be recognized by the ensuing characteristic encephalomalacia that often develops within the retracted tissue.

Currently, our standard postoperative protocol employs gadolinium to assess for residual, recurrent, and/or progressive tumor after vestibular schwannoma resection. Nodular enhancement within the postoperative IAC or cerebellopontine angle is suggestive of recurrent or residual tumor, whereas linear enhancement is presumed to represent postoperative granulation tissue (38). In the setting of subtotal resection, correlation with the operative report, if available, is crucial. Some investigators have suggested that high-resolution 3D T2-weighted sequences are sufficient for such follow-up evaluations (39,40). Kim et al (41), in a recent meta-analysis, found no significant difference between the sizes of recurrent tumors measured on contrast-enhanced and high-resolution T2-weighted images. Furthermore, normal postoperative enhancement can sometimes be confused for residual tumors (42). It is therefore possible that we may ultimately adjust our protocol to exclude the use of contrast material in some cases, particularly as concerns about gadolinium deposition are raised by referring providers and patients.

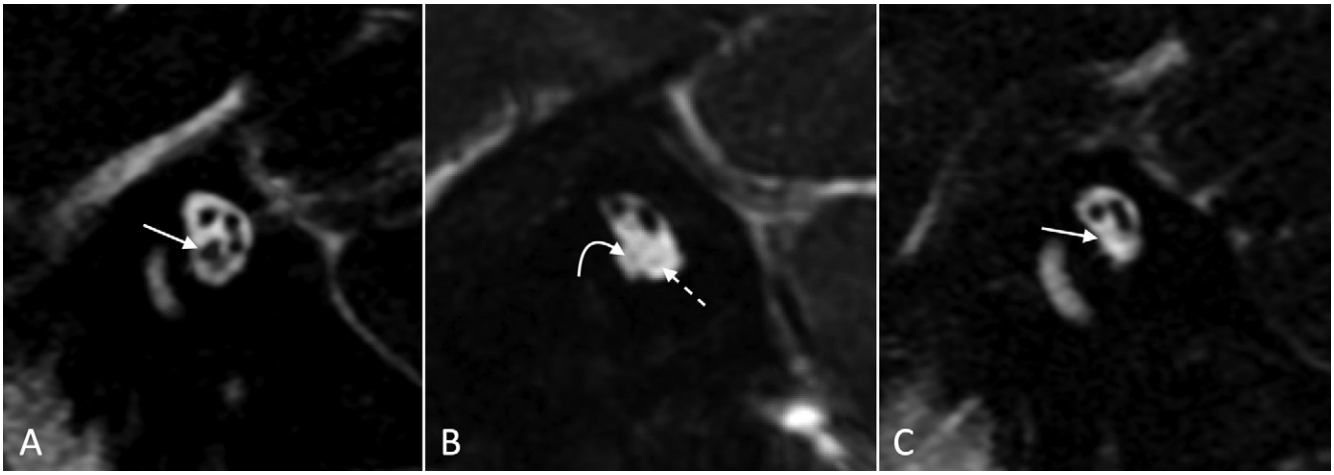

Figure 11: Reformatted oblique sagittal T2-weighted sampling perfection with application-optimized contrasts by using flip angle evolution, or SPACE, images show the spectrum of cochlear nerve anomalies. *A*, Normal cochlear nerve (arrow) in a 2-year-old boy is easily visualized in the anteroinferior internal auditory canal. *B*, Image demonstrates marked hypoplasia of the cochlear nerve (curved arrow) in an 8-year-old boy; the inferior vestibular nerve is also hypoplastic (straight arrow). *C*, Image shows an example of complete absence of the cochlear nerve (arrow) in a 2-year-old boy with sensorineural deafness.

Close attention should be paid to the membranous labyrinth in the postoperative setting. Early changes may include T1-hyperintense fluid, typically representing blood products or proteinaceous fluid. FLAIR hyperintensity might suggest the presence of proteinaceous fluid or inflammatory changes. The major concern, however, is that of cochlear luminal obliteration in light of recent interest in cochlear implant following vestibular schwannoma resection (43,44). Patients are prone to such changes after surgery, particularly after those performed with a translabyrinthine approach. Similar to labyrinthitis ossificans that develops from other causes (see the following section), cochlear obliteration appears as decreased, and ultimately absent, signal intensity with heavily T2-weighted sequences. Ossification can be confirmed with CT (45). Enhancement often precedes obliteration in the postoperative setting, often by a substantial period of time. Intense enhancement is seen a median of 5.4 months after surgery (interquartile range, 2.8–7.2 months); obliteration occurs a median of 16 months after vestibular schwannoma resection (interquartile range, 12.0–18.9 months) (46,47).

Labyrinthitis

Labyrinthitis refers to inflammation of the inner ear and a vast majority of cases are infectious, in which the offending agent may enter the inner ear by direct spread (ie, through adjacent structures such as the middle ear [tympanogenic] or meninges [meningogenic]) or through hematogenic seeding from a remote source (48). Among children, *Streptococcus* meningitis is the most common cause of labyrinthitis, and meningitic labyrinthitis is the most common cause of acquired sensorineural hearing loss (49). Meningitic labyrinthitis can spread into the inner ear through multiple routes, including by the cochlear aqueduct and modiolus (50). The associated labyrinthitis is usually bilateral. Tympanogenic infections, conversely, enter the inner ear through the oval and round windows and result in unilateral symptoms (51).

Detection of labyrinthitis is of upmost importance because of its proclivity to progress to labyrinthitis ossificans, a condition that may preclude successful cochlear implantation (discussed later) (52). Classically, MRI demonstrates increased FLAIR signal intensity, decreased T2 signal intensity, and enhancement within the affected areas of the labyrinth (Fig 7) (51,53). Faint intrinsic T1-hyperintense signal may also be seen, likely related to proteinaceous fluid. This is easily differentiated from hemorrhage, which does not demonstrate enhancement. However, results of early imaging may be negative; a normal examination does not exclude the clinical diagnosis of labyrinthitis. Nevertheless, enhancement does have prognostic value. In patients with meningitic labyrinthitis, the presence of enhancement is predictive of future hearing loss, with a sensitivity of 87% and a specificity of 100% (54).

The major imaging differential consideration is that of an intralabyrinthine schwannoma, which demonstrates similar characteristics. Some investigators have sought to use quantitative signal analysis to differentiate between these entities, although this technique is not used in our practice (55,56). Instead, we rely more on clinical and imaging findings. Intralabyrinthine schwannomas demonstrate more focal enhancement than labyrinthitis, have a soft-tissue filling defect on high-resolution T2-weighted images, and tend to enhance more avidly (Fig 8) (57).

Intrinsic T1-hyperintense signal within the labyrinth, conversely, represents presumed intralabyrinthine hemorrhage, also known as hemorrhagic labyrinthitis (Fig 9) (58,59). Often, the T1 signal intensity is patchy and lacks nodularity. Such cases tend to occur in specific clinical situations, such as in the context of trauma, surgery, disseminated intravascular coagulation, systemic lupus erythematosus, sickle cell disease, or the use of anticoagulants (60,61). Intralabyrinthine hemorrhage may also result from bacterial labyrinthitis. Patients typically present with profound sudden sensorineural hearing loss, from which they generally do not recover (62).

Autoimmune labyrinthitis is a known, albeit rare, subtype of labyrinthitis. Patients typically present with steroid-responsive fluctuating bilateral asymmetric sensorineural hearing loss and/or vestibular symptoms and often have other known autoimmune diseases such as ulcerative colitis. Contrary to Meniere disease,

which is usually unilateral, autoimmune labyrinthitis often affects both ears at once (63). MRI findings are similar to those of other causes of labyrinthitis, with avid enhancement of the labyrinthine structures and/or vestibular nerves (64). Although it is often a diagnosis of exclusion, some laboratory tests may support autoimmune labyrinthitis as a clinical consideration, including C-reactive protein level, erythrocyte sedimentation rate, and rheumatoid factor. Autoimmune labyrinthitis, like other forms of labyrinthitis, can progress to labyrinthitis ossificans (65).

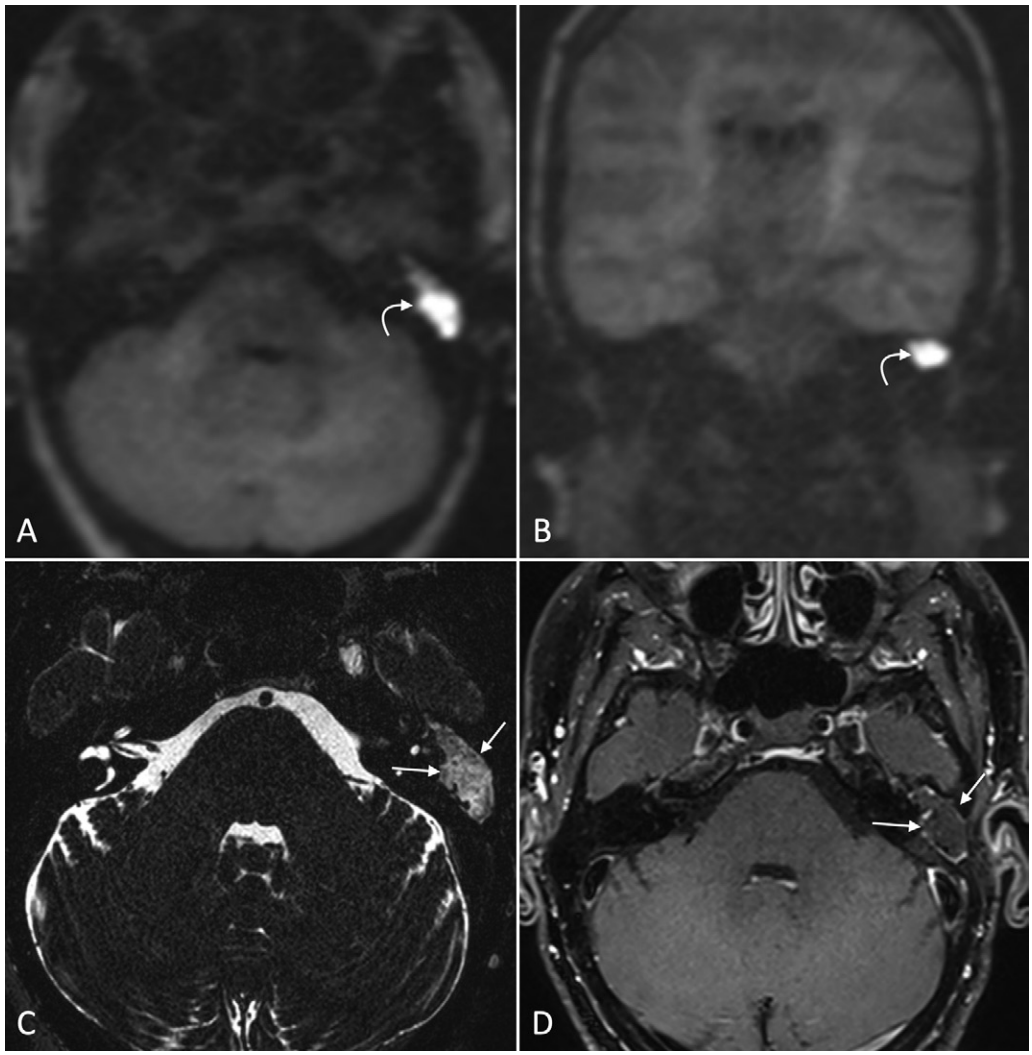

Figure 12: Recurrent cholesteatoma in a 49-year-old woman who underwent a canal wall up tympanomastoidectomy and ossicular chain reconstruction 10 years earlier for resection of a cholesteatoma. The patient has had recurrent pressure and a sensation of fluid in her ear. *A*, Axial and, *B*, coronal diffusion-weighted half-Fourier acquisition single-shot turbo spin-echo images demonstrate a focus of restricted diffusion (arrow) in her operative site, compatible with a recurrent cholesteatoma. *C*, Axial T2-weighted sampling perfection with application-optimized contrasts by using flip angle evolution (SPACE) image and, *D*, axial contrast-enhanced T1-weighted SPACE image show nonspecific soft-tissue signal intensity with faint peripheral enhancement (arrows), highlighting the usefulness of diffusion-weighted imaging.

Labyrinthitis Ossificans

As mentioned earlier, labyrinthitis ossificans results from inner ear inflammation, in which the membranous labyrinth is filled with ossific material (51). Although infection is the most common cause, numerous processes may result in labyrinthitis ossificans. Trauma, surgery, and inflammatory, autoimmune, and sickle cell disease have all been implicated (66,67). Patients often present with sensorineural hearing loss, which can be profound.

Classically, the progression to labyrinthitis ossificans occurs in a predictable pattern. Bacteria and/or leukocytes within the perilymphatic spaces are associated with a serofibrinous exudate, which leads to the proliferation of fibroblasts followed by the formation of osteoid matrix (68). These histopathologic changes are categorized into three distinct phases: acute, fibrous, and ossifying. The fibrous and ossifying phases can occur as early as 2 weeks and 2 months after infection, respectively (69).

Nonenhanced CT is useful in end-stage labyrinthitis ossificans, in which the ossific material is easily visualized. However, MRI can play a crucial role in the diagnosis of earlier and/or developing labyrinthitis ossificans, when CT imaging remains normal. Specifically, inner ear fibrosis can be detected with heavily T2-weighted sequences, which demonstrate decreased signal intensity within the affected labyrinthine structures (70). Inner ear enhancement may also be seen in the fibrous stage, though less avidly than that seen during acute labyrinthitis (71). During the ossifying phase, the affected structures are classically devoid of signal intensity on T2-weighted images and will no longer enhance (Fig 10). However, some overlap in imaging features can be seen, particularly between the fibrous and ossifying phases at MRI. CT may be useful in such cases to assess for inner ear ossification.

Labyrinthitis ossificans typically starts within the scala tympani in the basal turn of the cochlea, near the round window (72). This is because the cochlear aqueduct enters the basal turn near the round window and represents a conduit for spread of infection from the subarachnoid space in meningitis. From there, it progresses to the cochlear apex (73). However, any part of the membranous labyrinth can be involved. Postoperative labyrinthitis ossificans most commonly affects the basal turn of the cochlea,

vestibule, and semicircular canals. Mineralization patterns of labyrinthitis ossificans resulting from other risk factors are nonspecific and are not useful for determining the etiologic origins (74).

Cochlear Implantation Evaluation

Preprocedural imaging is crucial before placement of a cochlear implant. Temporal bone CT scans are primarily used to assess the bony structures, such as ensuring that the course of the facial nerve is not aberrant, particularly in patients with CHARGE syndrome, branchio-oto-renal syndrome, or dysplasia of the semicircular canals. The IAC diameter should also be noted at CT. A narrowed IAC (<3 mm) or cochlear aperture should alert radiologists to the possibility of vestibulocochlear nerve aplasia or deficiency (75,76). Nevertheless, MRI must be used for confirmation.

As mentioned earlier, the cisternal and canalicular segments of the vestibulocochlear and facial nerves are best scrutinized by using 3D high-resolution T2-weighted images acquired in an oblique plane perpendicular to the IAC. This is particularly important to evaluate in children with bilateral profound congenital hearing loss. Both absence and deficiency, which are generally defined as reduction in nerve caliber, are associated with sensorineural hearing loss. Absence of the nerve is almost always congenital and is generally viewed as an absolute contraindication to cochlear implantation (Fig 11). Deficiency, conversely, is only a relative contraindication, as such nerves can still sometimes successfully transmit neuronal impulses for hearing (77). Small or deficient nerves are typically congenital (hypoplasia) in nature. The average diameter of a normal cochlear nerve in the mid-to-distal IAC is 1.2 mm, similar in caliber to the facial nerve, and is larger than the superior and inferior vestibular nerves in the vast majority of cases (75,78). Comparison to the contralateral nerve can also be useful.

Preprocedural imaging should also be used to closely evaluate for cochlear anatomic variants, especially of cochlear aplasia and types of incomplete partition. Patients with all subtypes of incomplete partition may be candidates for cochlear implant. However, the deformities place them at risk for cerebrospinal fluid "gushers" and electrode misplacement during cochlear implantation and, consequently, at higher future risk for cerebrospinal fluid leak and meningitis. Incomplete partition type III, an anomaly present in X-linked congenital deafness, has the highest risk of potential complications; such cochleae are particularly prone to severe cerebrospinal fluid gushers and have a high likelihood of electrode misplacement. Incomplete partition type III deformities are characterized by complete absence of the modiolus and intact interscalar septa (79). Incomplete partition type I cochlea, in comparison, lack both the modiolus and interscalar septa; incomplete partition type II deformities are limited to the apical aspect of the modiolus and are commonly associated with enlarged vestibular aqueduct.

Finally, as earlier, labyrinthitis ossificans can make electrode placement challenging or even impossible and often leads to partial electrode array insertion (80). MRI is predictive of intraoperative cochlear obstruction, with a sensitivity of 94.1% and specificity of 87.5% (81). In patients with labyrinthitis, the urgency with which cochlear implantation is completed remains somewhat contentious. Some authors have argued for the use of regular MRI follow-up in patients with labyrinthitis, whereas others have opined that some patients should instead be directed to early cochlear implantation (80). Nevertheless, preprocedural MRI is typically recommended to optimize surgical preparation (82).

Cholesteatomas

Cholesteatomas are nonneoplastic expanding accumulations of keratinized squamous epithelium (83). Lesions are locally invasive and are capable of causing substantial destruction to the middle ear and adjacent structures. Complications include conductive hearing loss, facial paralysis, invasion of the labyrinth with subsequent sensorineural hearing loss, and a host of intracranial infection complications (84,85). Resection is typically used for treatment, by means of either canal wall down or canal wall up mastoidectomy. However, cholesteatomas are notoriously prone to reappear, with reported recurrence rates exceeding 7%–10% (86,87).

Nonenhanced CT is the modality most frequently used for initial diagnosis and preoperative planning. Although CT is highly sensitive for the detection of cholesteatomas, it is difficult to differentiate lesions from other soft-tissue attenuation abnormalities such as granulation tissue or mucosal thickening (88,89). Preoperatively, the presence of associated osseous erosion is a useful finding and is the hallmark CT finding of cholesteatomas. Postoperatively, however, nonenhanced CT suffers as a diagnostic tool. A well-aerated tympanomastoid cavity, which is rare in the postprocedural setting, is necessary to exclude residual lesions on a CT scan (90).

For many institutions, including ours, MRI is now the mainstay modality used to assess for residual or recurrent cholesteatomas. This technique is particularly useful in following up patients with prior canal wall up procedures that often include the construction of opaque cartilaginous tympanoplasties, precluding adequate clinical inspection of the middle ear. Previously, MRI evaluations depended on delayed contrast-enhanced images. Cholesteatomas are either nonenhancing or demonstrate thin peripheral enhancement, whereas postoperative and/or inflammatory tissue demonstrates homogeneous enhancement (91,92). In recent years, there has been a substantial rise in the use of non–echo planar diffusion-weighted imaging, which demonstrates conspicuous intralesional diffusion restriction (Fig 12). This had made MRI a powerful modality when assessing for recurrent lesions, with sensitivity, specificity, and accuracy reported to be 91%–94%, 88%–100%, and 92%–95%, respectively (82,91,93). As such, many institutions have now abandoned the use of delayed contrast-enhanced imaging (94). Others have even questioned whether MRI obviates a second-look surgery following canal wall up mastoidectomies, although diffusion-weighted imaging is limited in its ability to depict small (<3 mm) lesions and those with thin mural growth patterns (95).

False-positive findings do exist and are usually attributed to cerumen, abscesses, and scar tissue (96). Here, review of multiple other sequences is useful to supplement the evaluation for such mimickers. On apparent diffusion coefficient images, cholesteatomas tend to have lower signal than fluid and postoperative granulation tissue (97). On precontrast T1-weighted images, cholesteatomas demonstrate hypointense T1 signal, whereas cholesterol

granulomas are often hyperintense (98). T1- and T2-weighted images are also useful in anatomically localizing the signal abnormalities seen on diffusion-weighted images. Finally, the morphologic characteristics of any abnormalities should be considered. Wax in the external auditory canal, for example, tends to be linear and/or parallel in configuration (95).

Conclusion

MRI of the inner auditory canal and inner ear is characterized by a diverse array of pathologic conditions. Interpretation of such examinations requires optimized imaging protocols and a sound knowledge of the intricate anatomy. Radiologists must therefore familiarize themselves with the relevant anatomic variants and the diverse array of pathologic conditions that can be seen on these MRI scans. Furthermore, to optimize their usefulness to the ordering providers, radiologists should be well-versed in the expected pre- and postoperative findings related to the most commonly performed surgeries.

Disclosures of Conflicts of Interest: J.C.B. disclosed no relevant relationships. **M.L.C.** disclosed no relevant relationships. **J.I.L.** disclosed no relevant relationships.

References

1. Lane JI, Ward H, Witte RJ, Bernstein MA, Driscoll CLW. 3-T imaging of the cochlear nerve and labyrinth in cochlear-implant candidates: 3D fast recovery fast spin-echo versus 3D constructive interference in the steady state techniques. AJNR Am J Neuroradiol 2004;25(4):618–622.
2. van der Jagt MA, Brink WM, Versluis MJ, et al. Visualization of human inner ear anatomy with high-resolution MR imaging at 7T: initial clinical assessment. AJNR Am J Neuroradiol 2015;36(2):378–383.
3. van Egmond SL, Visser F, Pameijer FA, Grolman W. Ex vivo and in vivo imaging of the inner ear at 7 Tesla MRI. Otol Neurotol 2014;35(4):725–729.
4. Schmalbrock P. Comparison of three-dimensional fast spin echo and gradient echo sequences for high-resolution temporal bone imaging. J Magn Reson Imaging 2000;12(6):814–825.
5. Byun JS, Kim HJ, Yim YJ, et al. MR imaging of the internal auditory canal and inner ear at 3T: comparison between 3D driven equilibrium and 3D balanced fast field echo sequences. Korean J Radiol 2008;9(3):212–218.
6. Naganawa S, Koshikawa T, Fukatsu H, Ishigaki T, Fukuta T. MR cisternography of the cerebellopontine angle: comparison of three-dimensional fast asymmetrical spin-echo and three-dimensional constructive interference in the steady-state sequences. AJNR Am J Neuroradiol 2001;22(6):1179–1185.
7. Jung NY, Moon WJ, Lee MH, Chung EC. Magnetic resonance cisternography: comparison between 3-dimensional driven equilibrium with sensitivity encoding and 3-dimensional balanced fast-field echo sequences with sensitivity encoding. J Comput Assist Tomogr 2007;31(4):588–591.
8. Bertot B, Steele WJ, Boghani Z, Britz G. Diagnostic Dilemma: Cerebellopontine Angle Lipoma Versus Dermoid Cyst. Cureus 2017;9(11):e1894.
9. Filli L, Huber A, Husain NA. Symptomatic Lipoma of the Internal Auditory Canal: CT and MRI Findings. A Case Report. Neuroradiol J 2014;27(4):479–481.
10. van Egmond SL, Stegeman I, Grolman W, Aarts MCJ. A Systematic Review of Non-Echo Planar Diffusion-Weighted Magnetic Resonance Imaging for Detection of Primary and Postoperative Cholesteatoma. Otolaryngol Head Neck Surg 2016;154(2):233–240.
11. De Foer B, Vercruysse JP, Bernaerts A, et al. Detection of postoperative residual cholesteatoma with non-echo-planar diffusion-weighted magnetic resonance imaging. Otol Neurotol 2008;29(4):513–517.
12. Felici F, Scemama U, Bendahan D, et al. Improved Assessment of Middle Ear Recurrent Cholesteatomas Using a Fusion of Conventional CT and Non-EPI-DWI MRI. AJNR Am J Neuroradiol 2019;40(9):1546–1551.
13. Burmeister HP, Baltzer PA, Dietzel M, et al. Identification of the nervus intermedius using 3T MR imaging. AJNR Am J Neuroradiol 2011;32(3):460–464.
14. Valvassori GE, Palacios E. Magnetic resonance imaging of the internal auditory canal. Top Magn Reson Imaging 2000;11(1):52–65.
15. Benson JC, Eckel L, Guerin J, et al. Review of Temporal Bone Microanatomy : Aqueducts, Canals, Clefts and Nerves. Clin Neuroradiol 2020;30(2):209–219.
16. Juliano AF, Ginat DT, Moonis G. Imaging review of the temporal bone: part I. Anatomy and inflammatory and neoplastic processes. Radiology 2013;269(1):17–33.
17. Lane JI, Witte RJ, Bolster B, Bernstein MA, Johnson K, Morris J. State of the art: 3T imaging of the membranous labyrinth. AJNR Am J Neuroradiol 2008;29(8):1436–1440.
18. Naganawa S, Sugiura M, Kawamura M, Fukatsu H, Sone M, Nakashima T. Imaging of endolymphatic and perilymphatic fluid at 3T after intratympanic administration of gadolinium-diethylene-triamine pentaacetic acid. AJNR Am J Neuroradiol 2008;29(4):724–726.
19. Lopez-Escamez JA, Attyé A. Systematic review of magnetic resonance imaging for diagnosis of Meniere disease. J Vestib Res 2019;29(2-3):121–129.
20. Celis-Aguilar E, Lassaletta L, Torres-Martín M, et al. The molecular biology of vestibular schwannomas and its association with hearing loss: a review. Genet Res Int 2012;2012:856157.
21. Lin D, Hegarty JL, Fischbein NJ, Jackler RK. The prevalence of "incidental" acoustic neuroma. Arch Otolaryngol Head Neck Surg 2005;131(3):241–244.
22. Marinelli JP, Lohse CM, Carlson ML. Incidence of Vestibular Schwannoma over the Past Half-Century: A Population-Based Study of Olmsted County, Minnesota. Otolaryngol Head Neck Surg 2018;159(4):717–723.
23. Lees KA, Tombers NM, Link MJ, et al. Natural History of Sporadic Vestibular Schwannoma: A Volumetric Study of Tumor Growth. Otolaryngol Head Neck Surg 2018;159(3):535–542.
24. Lovato A, García Ibañez E, García Ibañez L, de Filippis C. Tumor growth rate: A new prognostic indicator of hearing preservation in vestibular schwannoma surgery. Laryngoscope 2019;129(10):2378–2383.
25. Goddard JC, Schwartz MS, Friedman RA. Fundal fluid as a predictor of hearing preservation in the middle cranial fossa approach for vestibular schwannoma. Otol Neurotol 2010;31(7):1128–1134.
26. Benech F, Perez R, Fontanella MM, Morra B, Albera R, Ducati A. Cystic versus solid vestibular schwannomas: a series of 80 grade III-IV patients. Neurosurg Rev 2005;28(3):209–213.
27. Bhadelia RA, Tedesco KL, Hwang S, et al. Increased cochlear fluid-attenuated inversion recovery signal in patients with vestibular schwannoma. AJNR Am J Neuroradiol 2008;29(4):720–723.
28. Silverstein H. Labyrinthine tap as a diagnostic test for acoustic neurinoma. Otolaryngol Clin North Am 1973;6(1):229–244.
29. Lee IH, Kim HJ, Chung WH, et al. Signal intensity change of the labyrinth in patients with surgically confirmed or radiologically diagnosed vestibular schwannoma on isotropic 3D fluid-attenuated inversion recovery MR imaging at 3 T. Eur Radiol 2010;20(4):949–957.
30. Yamazaki M, Naganawa S, Kawai H, Nihashi T, Fukatsu H, Nakashima T. Increased signal intensity of the cochlea on pre- and post-contrast enhanced 3D-FLAIR in patients with vestibular schwannoma. Neuroradiology 2009;51(12):855–863.
31. Yoshida T, Sugiura M, Naganawa S, Teranishi M, Nakata S, Nakashima T. Three-dimensional fluid-attenuated inversion recovery magnetic resonance imaging findings and prognosis in sudden sensorineural hearing loss. Laryngoscope 2008;118(8):1433–1437.
32. Lin EP, Crane BT. The Management and Imaging of Vestibular Schwannomas. AJNR Am J Neuroradiol 2017;38(11):2034–2043.
33. Rosahl S, Bohr C, Lell M, Hamm K, Iro H. Diagnostics and therapy of vestibular schwannomas - an interdisciplinary challenge. GMS Curr Top Otorhinolaryngol Head Neck Surg 2017;16:Doc03.
34. Suryanarayanan R, Ramsden RT, Saeed SR, et al. Vestibular schwannoma: role of conservative management. J Laryngol Otol 2010;124(3):251–257.
35. Cueva RA, Chole RA. Maximizing Exposure of the Internal Auditory Canal Via the Retrosigmoid Approach: An Anatomical, Radiological, and Surgical Study. Otol Neurotol 2018;39(7):916–921.
36. Carlson ML, Tombers NM, Driscoll CLW, et al. Clinically significant intratumoral hemorrhage in patients with vestibular schwannoma. Laryngoscope 2017;127(6):1420–1426.
37. Silk PS, Lane JI, Driscoll CL. Surgical approaches to vestibular schwannomas: what the radiologist needs to know. RadioGraphics 2009;29(7):1955–1970.
38. Carlson ML, Van Abel KM, Driscoll CL, et al. Magnetic resonance imaging surveillance following vestibular schwannoma resection. Laryngoscope 2012;122(2):378–388.
39. Williams JC, Carr CM, Eckel LJ, et al. Utility of Noncontrast Magnetic Resonance Imaging for Detection of Recurrent Vestibular Schwannoma. Otol Neurotol 2018;39(3):372–377.
40. Buch K, Juliano A, Stankovic KM, Curtin HD, Cunnane MB. Noncontrast vestibular schwannoma surveillance imaging including an MR cisternographic sequence: is there a need for postcontrast imaging? J Neurosurg 2018;131(2):549–554.
41. Kim DH, Lee S, Hwang SH. Non-contrast Magnetic Resonance Imaging for Diagnosis and Monitoring of Vestibular Schwannomas: A Systematic Review and Meta-analysis. Otol Neurotol 2019;40(9):1126–1133.
42. Zaidi HA, Chowdhry SA, Wilson DA, Spetzler RF. The dilemma of early postoperative magnetic resonance imaging: when efficiency compromises accuracy: case report. Neurosurgery 2014;74(3):E335–E340; discussion E340.

43. Hassepass F, Arndt S, Aschendorff A, Laszig R, Wesarg T. Cochlear implantation for hearing rehabilitation in single-sided deafness after translabyrinthine vestibular schwannoma surgery. Eur Arch Otorhinolaryngol 2016;273(9):2373–2383.
44. Osborn HA, Yeung R, Lin VYW. Delayed cochlear implantation after surgical labyrinthectomy. J Laryngol Otol 2012;126(1):63–65.
45. Raut V, Toner JG. Cochlear implantation in the obliterated cochlea. Clin Otolaryngol Allied Sci 2002;27(3):147–152.
46. Erbele ID, Miller LS, Mankekar G, et al. Cochlear Enhancement May Precede Cochlear Obliteration After Vestibular Schwannoma Excision. Otol Neurotol 2020;41(2):202–207.
47. Feng Y, Lane JI, Lohse CM, Carlson ML. Pattern of cochlear obliteration after vestibular Schwannoma resection according to surgical approach. Laryngoscope 2020;130(2):474–481.
48. Mattiola LR, Makowiecky M, Salles CEG, Cardoso MP, Cahali S. Labyrinthitis Ossificans. Report of One Case and Literature Review. Int Arch Otorhinolaryngol 2008;12(2):300–302. http://www.arquivosdeorl.org.br/conteudo/acervo_eng.asp?id=530.
49. Huang BY, Zdanski C, Castillo M. Pediatric sensorineural hearing loss, part 2: syndromic and acquired causes. AJNR Am J Neuroradiol 2012;33(3):399–406.
50. Benson JC, Diehn F, Passe T, et al. The Forgotten Second Window: A Pictorial Review of Round Window Pathologies. AJNR Am J Neuroradiol 2020;41(2):192–199.
51. Campion T, Taranath A, Pinelli L, et al. Imaging of temporal bone inflammations in children: a pictorial review. Neuroradiology 2019;61(9):959–970.
52. Aschendorff A, Klenzner T, Laszig R. Deafness after bacterial meningitis: an emergency for early imaging and cochlear implant surgery. Otolaryngol Head Neck Surg 2005;133(6):995–996.
53. Lee SJ, Lee SA, Kim BG, Hong HS, Lee JY, Lee JD. Feasibility of magnetic resonance imaging in the differential diagnosis of isolated acute audiovestibular loss. J Vestib Res 2018;28(5-6):385–391.
54. Kopelovich JC, Germiller JA, Laury AM, Shah SS, Pollock AN. Early prediction of postmeningitic hearing loss in children using magnetic resonance imaging. Arch Otolaryngol Head Neck Surg 2011;137(5):441–447.
55. Bae YJ, Song JJ, Choi BS, Kang Y, Kim JH, Koo JW. Differentiation Between Intralabyrinthine Schwannoma and Contrast-enhancing Labyrinthitis on MRI: Quantitative Analysis of Signal Intensity Characteristics. Otol Neurotol 2018;39(8):1045–1052.
56. Peng R, Chow D, De Seta D, Lalwani AK. Intensity of gadolinium enhancement on MRI is useful in differentiation of intracochlear inflammation from tumor. Otol Neurotol 2014;35(5):905–910.
57. Salzman KL, Childs AM, Davidson HC, Kennedy RJ, Shelton C, Harnsberger HR. Intralabyrinthine schwannomas: imaging diagnosis and classification. AJNR Am J Neuroradiol 2012;33(1):104–109.
58. Kim DS, Park DW, Kim TY, et al. Characteristic MR findings suggesting presumed labyrinthine hemorrhage. Acta Otolaryngol 2017;137(12):1226–1232.
59. Park JJ, Jeong SW, Lee JW, Han SJ. A Case of Sudden Deafness with Intralabyrinthine Hemorrhage Intralabyrinthine Hemorrhage and Sudden Deafness. J Audiol Otol 2015;19(3):178–181.
60. Dubrulle F, Kohler R, Vincent C, Puech P, Ernst O. Differential diagnosis and prognosis of T1-weighted post-gadolinium intralabyrinthine hyperintensities. Eur Radiol 2010;20(11):2628–2636.
61. Cervantes SS, Barrs DM. Sudden Sensorineural Hearing Loss Associated With Intralabyrinthine Hemorrhage. Otol Neurotol 2015;36(8):e134–e135.
62. Vivas EX, Panella NJ, Baugnon KL. Spontaneous Labyrinthine Hemorrhage: A Case Series. Otolaryngol Head Neck Surg 2018;159(5):908–913.
63. Agrup C. Immune-mediated audiovestibular disorders in the paediatric population: a review. Int J Audiol 2008;47(9):560–565.
64. Hwang M, Zuccoli G. Rapidly Destructive Autoimmune Labyrinthitis Associated With Ulcerative Colitis. Pediatr Neurol 2015;53(4):375–376.
65. Benson AG. Labyrinthitis ossificans secondary to autoimmune inner ear disease: a previously unreported condition. Otolaryngol Head Neck Surg 2010;142(5):772–773.
66. Swartz JD, Mandell DM, Faerber EN, et al. Labyrinthine ossification: etiologies and CT findings. Radiology 1985;157(2):395–398.
67. Lin HY, Fan YK, Wu KC, Shu MT, Yang CC, Lin HC. The incidence of tympanogenic labyrinthitis ossificans. J Laryngol Otol 2014;128(7):618–620.
68. Vyas S, Bhatia V, Panda NK, Singh P, Khandelwal N. Labyrinthitis ossificans after meningitis: Superiority of high-resolution magnetic resonance imaging in demonstration of disease extent compared to high-resolution computed tomography. J Neurosci Rural Pract 2016;7(2):327–329.
69. Hegarty JL, Patel S, Fischbein N, Jackler RK, Lalwani AK. The value of enhanced magnetic resonance imaging in the evaluation of endocochlear disease. Laryngoscope 2002;112(1):8–17.
70. Booth TN, Roland P, Kutz JW Jr, Lee K, Isaacson B. High-resolution 3-D T2-weighted imaging in the diagnosis of labyrinthitis ossificans: emphasis on subtle cochlear involvement. Pediatr Radiol 2013;43(12):1584–1590.
71. Lemmerling MM, De Foer B, Verbist BM, VandeVyver V. Imaging of inflammatory and infectious diseases in the temporal bone. Neuroimaging Clin N Am 2009;19(3):321–337.
72. Green JD Jr, Marion MS, Hinojosa R. Labyrinthitis ossificans: histopathologic consideration for cochlear implantation. Otolaryngol Head Neck Surg 1991;104(3):320–326.
73. Coelho DH, Roland JT Jr. Implanting obstructed and malformed cochleae. Otolaryngol Clin North Am 2012;45(1):91–110.
74. Buch K, Baylosis B, Fujita A, et al. Etiology-Specific Mineralization Patterns in Patients with Labyrinthitis Ossificans. AJNR Am J Neuroradiol 2019;40(3):551–557.
75. Glastonbury CM, Davidson HC, Harnsberger HR, Butler J, Kertesz TR, Shelton C. Imaging findings of cochlear nerve deficiency. AJNR Am J Neuroradiol 2002;23(4):635–643.
76. Fatterpekar GM, Mukherji SK, Alley J, Lin Y, Castillo M. Hypoplasia of the bony canal for the cochlear nerve in patients with congenital sensorineural hearing loss: initial observations. Radiology 2000;215(1):243–246.
77. Gupta SS, Maheshwari SR, Kirtane MV, Shrivastav N. Pictorial review of MRI/CT Scan in congenital temporal bone anomalies, in patients for cochlear implant. Indian J Radiol Imaging 2009;19(2):99–106.
78. Verbist BM. Imaging of sensorineural hearing loss: a pattern-based approach to diseases of the inner ear and cerebellopontine angle. Insights Imaging 2012;3(2):139–153.
79. Sennaroğlu L, Bajin MD. Classification and Current Management of Inner Ear Malformations. Balkan Med J 2017;34(5):397–411.
80. Philippon D, Bergeron F, Ferron P, Bussières R. Cochlear implantation in postmeningitic deafness. Otol Neurotol 2010;31(1):83–87.
81. Isaacson B, Booth T, Kutz JW Jr, Lee KH, Roland PS. Labyrinthitis ossificans: how accurate is MRI in predicting cochlear obstruction? Otolaryngol Head Neck Surg 2009;140(5):692–696.
82. Durisin M, Bartling S, Arnoldner C, et al. Cochlear osteoneogenesis after meningitis in cochlear implant patients: a retrospective analysis. Otol Neurotol 2010;31(7):1072–1078.
83. Kuo CL. Etiopathogenesis of acquired cholesteatoma: prominent theories and recent advances in biomolecular research. Laryngoscope 2015;125(1):234–240.
84. Fan X, Liu Z, Ding C, Chang Z, Ma Q. The value of turbo spin-echo diffusion-weighted imaging apparent diffusion coefficient in the diagnosis of temporal bone cholesteatoma. Clin Radiol 2019;74(12):977.e1–977.e7.
85. Gulati M, Gupta S, Prakash A, Garg A, Dixit R. HRCT imaging of acquired cholesteatoma: a pictorial review. Insights Imaging 2019;10(1):92.
86. Ajalloueyan M. Experience with surgical management of cholesteatomas. Arch Otolaryngol Head Neck Surg 2006;132(9):931–933.
87. Vartiainen E, Nuutinen J. Long-term results of surgical treatment in different cholesteatoma types. Am J Otol 1993;14(5):507–511.
88. Baráth K, Huber AM, Stämpfli P, Varga Z, Kollias S. Neuroradiology of cholesteatomas. AJNR Am J Neuroradiol 2011;32(2):221–229.
89. Khan MI, Patel S, Dasgupta K. Is HRCT Temporal Bone Necessary in All Cases of Active Squamous Chronic Otitis Media? Indian J Otolaryngol Head Neck Surg 2019;71(Suppl 2):1212–1216.
90. Jindal M, Riskalla A, Jiang D, Connor S, O'Connor AF. A systematic review of diffusion-weighted magnetic resonance imaging in the assessment of postoperative cholesteatoma. Otol Neurotol 2011;32(8):1243–1249.
91. Gouda M, Nasr WF, Abd Elbary ME-S, Razek MMA. MRI as an Alternative to Second Look Mastoid Surgery. Indian J Otolaryngol Head Neck Surg 2018;70(3):410–414.
92. Vaid S, Kamble Y, Vaid N, et al. Role of magnetic resonance imaging in cholesteatoma: the Indian experience. Indian J Otolaryngol Head Neck Surg 2013;65(Suppl 3):485–492.
93. Foti G, Beltramello A, Minerva G, et al. Identification of residual-recurrent cholesteatoma in operated ears: diagnostic accuracy of dual-energy CT and MRI. Radiol Med (Torino) 2019;124(6):478–486.
94. De Foer B, Vercruysse JP, Bernaerts A, et al. Middle ear cholesteatoma: non-echo-planar diffusion-weighted MR imaging versus delayed gadolinium-enhanced T1-weighted MR imaging--value in detection. Radiology 2010;255(3):866–872.
95. Lingam RK, Nash R, Majithia A, Kalan A, Singh A. Non-echoplanar diffusion weighted imaging in the detection of post-operative middle ear cholesteatoma: navigating beyond the pitfalls to find the pearl. Insights Imaging 2016;7(5):669–678.
96. Akkari M, Gabrillargues J, Saroul N, et al. Contribution of magnetic resonance imaging to the diagnosis of middle ear cholesteatoma: analysis of a series of 97 cases. Eur Ann Otorhinolaryngol Head Neck Dis 2014;131(3):153–158.
97. Lingam RK, Khatri P, Hughes J, Singh A. Apparent diffusion coefficients for detection of postoperative middle ear cholesteatoma on non-echo-planar diffusion-weighted images. Radiology 2013;269(2):504–510.
98. Fukuda A, Morita S, Harada T, et al. Value of T1-weighted Magnetic Resonance Imaging in Cholesteatoma Detection. Otol Neurotol 2017;38(10):1440–1444.